JOURNAL OF SOLID STATE CHEMISTRY 114, 271–276 (1995)

Positive Mixed Cation Effect in $Ag/TlSO_4$ Compositions and Phase Diagram for the Ag_2SO_4–Tl_2SO_4 System

Yanjia Lu[1] and E. A. Secco[2]

Chemistry Department, St. Francis Xavier University, Antigonish, Nova Scotia, Canada B2G 1C0

Received July 6, 1993; in revised form May 19, 1994; accepted May 20, 1994

The ac conductivity data for the binary system Ag_2SO_4–Tl_2SO_4 are presented and interpreted in terms of a positive mixed cation effect on cation conductivity that has features in common with the positive mixed alkali/cation effects observed for Na_2SO_4–Rb_2SO_4 and Ag_2SO_4–Rb_2SO_4 systems, respectively. The data point to other factors, such as ion–ion interactions, bonding, or "lattice loosening," that can promote ionic conductivity in isomorphous structure sulfates along with the larger isovalent guest-ion-free volume contribution. The relatively constant activation energy for ionic conductivity, $Q_c = 45 \pm 5$ kJ/mole, indicates a quasi-equal intersite electrostatic potential energy for the mobile cation in the hexagonal structure and indicates that the defect formation enthalpy term is zero or negligible. The ion transport mechanism is interpreted to be of the percolation type with structural connectivity being the critical parameter. The DSC calorimetry data show interesting solid phase transition behavior. The dependence of the solid phase transition enthalpy, ΔH_t, on composition is presented, along with the complete phase diagram for the Ag_2SO_4–$TlSO_4$ system.

INTRODUCTION

The first indications of a positive mixed cation effect were observed in a preliminary study on (Ag, K)SO_4 compositions (1). This was followed by a more detailed study on the (Na, Rb)SO_4 system which reported a positive mixed alkali effect (2) and more recently by an in-depth study on the positive mixed cation effect in the (Ag,Rb)SO_4 system (3). Similar behavior has also been reported recently on the ion conductivity of (Ag^+,Na^+)-nitrite sodalites (4). The positive mixed cation/alkali effect is now recognized as a genuine effect, in strong contrast to the well-established negative mixed alkali effect observed in disilicate glasses (5, 6), β-aluminas, and β-gallate (7).

The qualitative resemblance between the logarithm conductivity (σT) versus T^{-1} plot for ionic solids undergoing transition to a high conductivity phase and the site percolation probability function, i.e., the $P(p)$ plot (8, 9), suggests a percolation model for ion transport. The P versus p curve describes the function $P(p)$, where P is the percolation probability or the fraction of the system taken up by the percolation path and p represents the probability that a site is unblocked or the probability of intersite connectivity. That is, at the phase transition or the structural percolation threshold the number of intersite channel connectivities or the percolation probability in the network structure increases sharply, giving rise to the observed abrupt jump in ion conductivity.

Fast-ion conduction is solids is considered a paradigm for a structure–property relation, where the ionic conductivity σ is a composite quantity $\sigma = nqu$ with n the concentration of the charge carriers q, and u the mobility of these carriers. The carrier mobility is related to a set of energetically favorable sites in the structure that are not normally occupied. The concomitant volume expansion for the sulfates, i.e., $+\Delta V$ of 3–4.5%, with the phase transition implied, *ceteris paribus*, that structure "free" volume was a major factor contributing to conductivity enhancement in these compounds (2, 10–12) and in the lower density of the glass phase relative to the crystal phase for Na^+, Cu^+, and Li^+ ion conductivity compositions (10, 13–15). The conductivity jump-free volume correlation is not obtained, however, for AgI, TlI, and CsCl, where the structure factor overrides the volume factor. Furthermore, recent studies incorporating the quasi-equal radius Rb^+ (166 pm) and Tl^+ (164 pm) in Ag_2SO_4 (16) failed to support the conductivity-free volume relationship in the isomorphous hexagonal structure space group $P6_3/mmc$ of α-Ag_2SO_4, α-Rb_2SO_4, and α-Tl_2SO_4. Also, the ionic conductivity of Tl_2SO_4 is $\sim 10^3$ times higher than that of Rb_2SO_4, and is of the same order of magnitude as that of Ag_2SO_4 despite the larger mass of Tl^+ (factor of 2) and its larger radius, i.e., 164 pm versus 129 pm for CN = 6(17). These inconsistencies point to factors other than the geometry of the anion array and structure free volume as major contributors to fast-ion conductivity, such as cation–anion interactions, vibra-

[1]In partial fulfillment for M.Sc. degree.

[2]To whom correspondence should be addressed.

0022-4596/95 $6.00

tional amplitudes of neighboring ions, and lattice resiliency.

The chemistry of Tl^+ bears some resemblance to that of Ag^+ (18) and of the alkali metals, especially Rb^+ (19), with differences linked to the lone electron pair of Tl^+. It was thought that α-Tl_2SO_4 provided an opportunity to probe the modality of fast cation conductivity in the hexagonal structure isomorphous with α-Ag_2SO_4, paralleling the study for $Rb/AgSO_4$ compositions by focusing on the substitutional effect of the presence of Tl^+ on Ag_2SO_4 with regard to the vibrational amplitude of the guest ion, the mass factor, and cation–anion interaction or bonding characteristics involving the outer electron configurations, viz., Ag^+-$4d^{10}$, Tl^+-$5d^{10}6s^2$, and Rb^+-$3d^{10}4s^2p^6$, where each compound has an isostructural SO_4^{2-} anion framework in the high temperature α-phase. This paper presents ac electrical conductivity data, solid–solid phase transition enthalpies (ΔH_t), and the subsolidus phase diagram for the Ag_2SO_4–Tl_2SO_4 system, along with mechanistic and structural interpretations.

EXPERIMENTAL

The chemicals used, Ag_2SO_4 and Tl_2SO_4, were Alfa Products (Thiokol/Ventron) with stated purities 99.9% and 99.5%, respectively. Samples of 99.0% grade Tl_2SO_4 supplied by American Smelting and Refining Co. (ASARCO) that were recrystallized in distilled H_2O gave the same results for the conductivity and DSC measurements as the Alfa reagents. All studied samples were prepared by grinding well manually, fusing the requisite compositions in air 50–70 K above melting (20) in a porcelain crucible and gradually cooling in the furnace to room temperature. The melting temperatures of Ag_2SO_4–Tl_2SO_4 compositions obtained from differential scanning calorimetry (DSC) are also presented (see Fig. 4).

The enthalpies of solid–solid phase transitions were evaluated with the differential scanning calorimeter (DSC) accessory to the DuPont 1090B thermal analyzer module equipped with disk memory and data analyzer. The samples, either an uncompressed fused portion or a compressed mass encapsulated in gold pans, were bathed under flowing (ultrapure) N_2. The calorimeter was calibrated up to 600°C using the enthalpies of fusion or transition for Li_2SO_4, KNO_3, Ag_2SO_4, $NaNO_3$, and *p*-nitroaniline as reference values.

The ac electrical conductivity measurements were done on compressed ground-particle discs, prepared under a pressure of ~15 MPa for 30 min in a stainless steel conductivity cell, and following the procedure described earlier (3, 10). The disc 1 cm in diameter and 1–2 mm in thickness, both surfaces of which were touched with graphite (Dag #154 Acheson), was maintained by a spring-loaded support between stainless steel leads using two polished Pt discs as electrodes. Each sample was preconditioned in the cell at 100°C under reduced pressure (~10^{-3} Torr) for 10–12 hr prior to measurement at 1 kHz. The conductivity was measured by continuous automatic recording with a GenRad 1688 LC Digibridge interfaced to an Apple IIe microcomputer and an Epson PX-85 printer at a heating and cooling rate of ~1°C min^{-1} unless otherwise stated. Temperature was monitored by a standardized chromel–alumel thermocouple with a Hewlett–Packard 3478A multimeter. This conductivity technique has been confirmed over a range of frequencies by a more sophisticated impedance setup in an independent laboratory (16).

RESULTS AND DISCUSSION

A. DSC and Transition Enthalpies, Phase Diagram

Typical DSC heat and cool traces are given in Figs. 1 and 2. The DSC trace for the compound $AgTlSO_4$ was reported earlier (16). The $\beta \leftrightarrow \alpha$, orthorhombic ↔ hexagonal transition in Tl_2SO_4 occurs at 497 ± 2°C, (Fig. 2), in good agreement with 500 ± 2°C (23). The low transition enthalpy ΔH_t = 890 ± 60 J/mole for Tl_2SO_4 is equal to the ΔH_t for the $\beta \leftrightarrow \alpha$, orthorhombic ↔ cubic, TlI transition (24). The DSC cool trace for freshly crystallized Tl_2SO_4 shows an extra exotherm near 450°C along with the expected one near 490°C, in contrast to the single exotherm at 497°C on the cool trace of the same sample 3 months later. The 450°C exotherm is attributed to a metastable state already reported (23, 25, 26). The negligible hysteresis for the $\beta \leftrightarrow \alpha$ transition in the absence of the metasta-

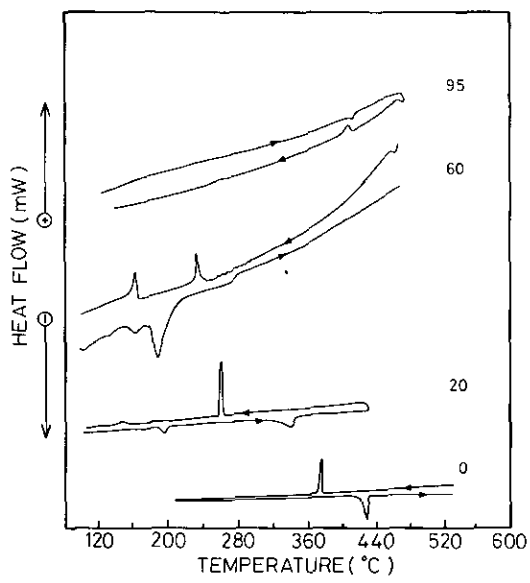

FIG. 1. DSC heat and cool traces for Ag_2SO_4–Tl_2SO_4 system in mol% Tl_2SO_4: 0, 20, 60, 95.

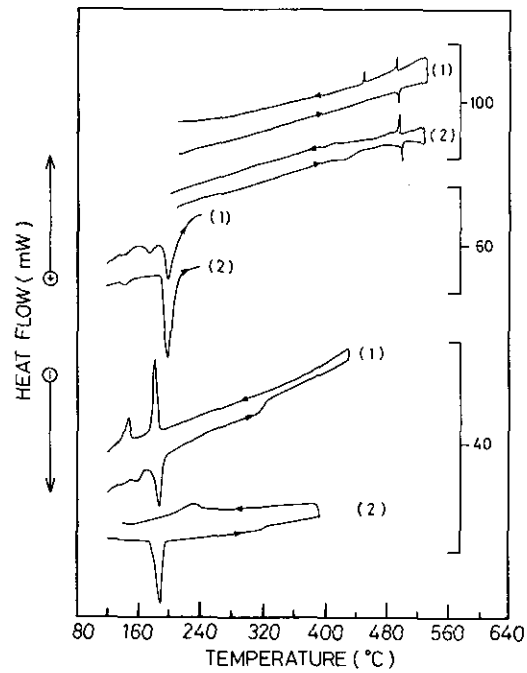

FIG. 2. DSC heat and cool traces for Ag_2SO_4–Tl_2SO_4 system in mol% Tl_2SO_4: 40, 60, 100, where 1 and 2 represent the effects of aging on 40 and 100, and the effects of pressure on 60.

ble state is consistent with the conductivity behavior for compressed disc sample. The effects of aging exhibited on the 40 mole% and of pressure on the 60 mole% Tl_2SO_4 (traces 1 and 2 in Fig. 2, respectively) illustrate the relaxation and transformation behavior of these metastable states.

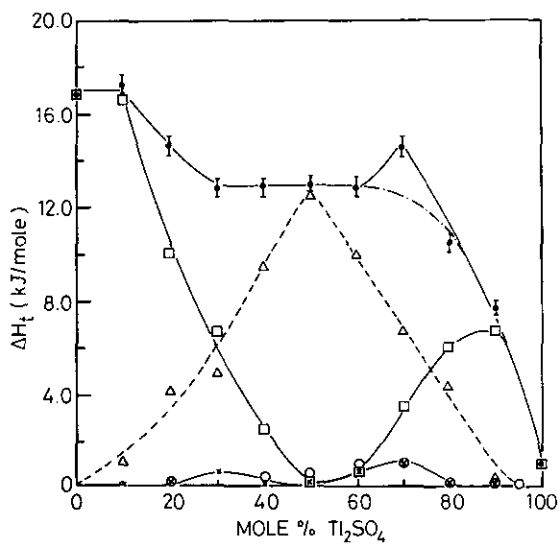

FIG. 3. Plots of ΔH_t for various phase transitions versus composition for the Ag_2SO_4–Tl_2SO_4 system: -(X) 145°C, (○) 175°C, (△) 193°C, (□) A_{ss}, B_{ss}, (↕) sum total.

Plots of the transition ΔH_t versus mole fraction Tl_2SO_4 for the observed endotherms are presented in Fig. 3. The 193°C endotherm is due to the $\beta \leftrightarrow \alpha$ transition of $AgTlSO_4$ (16). The weak endotherms at 145 and 175°C are assigned to dissociations of weakly associated 1 : 1 complexes or clusters involving β-$AgTlSO_4$, with β-Ag_2SO_4 or β-Tl_2SO_4 parallelling the behavior of $NaCsSO_4$ (25). The more stable complex appears at 70 mole %, as indicated by the maximum ΔH_t sum relative to the constant ΔH_t sum of 12.6 kJ/mole. The dotted–dashed line between 60 and 80 mole % represents the anticipated mirror image continuation of 10–30 mole % behavior. From the DSC thermal effects traces and their ΔH_t values (Figs. 1–3), we construct and label the subsolidus phase diagram for the Ag_2SO_4–Tl_2SO_4 system (Fig. 4). While both endothermic effects at 145 and 175°C are given in Fig. 4, it should be noted that these two effects never appeared on the same DSC trace and are taken from different sample preparations. Only two endotherms appeared on a given DSC trace, viz., 145 and 193°C, or 175 and 193°C. We assign the invariant temperature at 345°C to a three-phase system, viz., B_{ss} + complex + β-Tl_2SO_4. The solid–liquid portion of our phase diagram is at distinct variance with the solid–liquid diagram of Dombrovskaya (20). The solid–liquid data indicate the peak melting temperatures and the bars indicate the full width of the single melting endotherm. The persistence of the

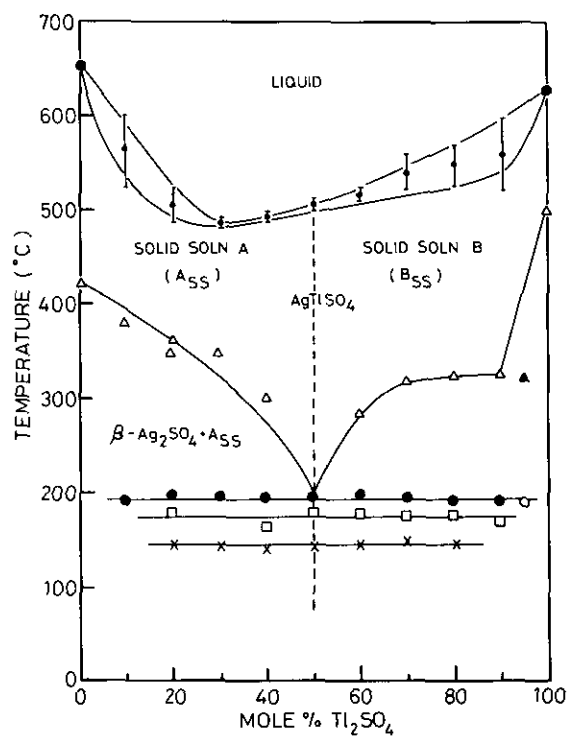

FIG. 4. Phase diagram for Ag_2SO_4–Tl_2SO_4 system.

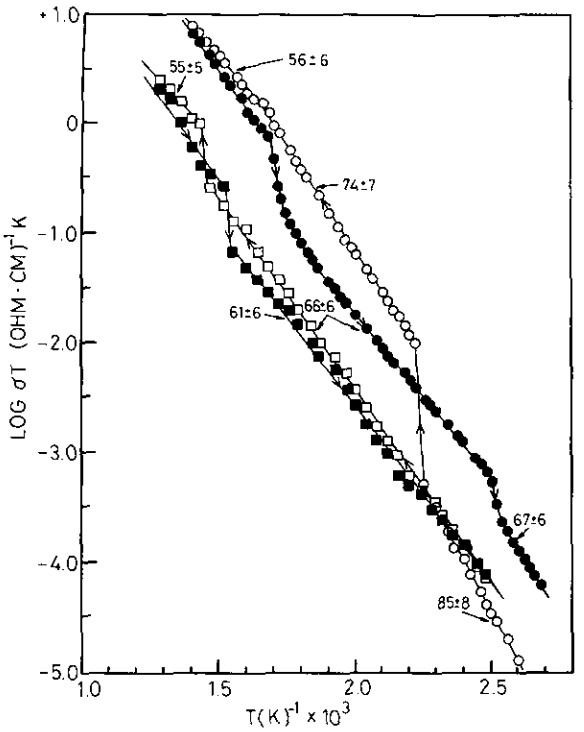

FIG. 5. Typical heat and cool model plots of logarithm (σT) versus $T(K)^{-1}$ for Ag_2SO_4–Tl_2SO_4 system: pure Ag_2SO_4, (□) heat, (■) cool; 90 : 10 mole ratio Ag_2SO_4–Tl_2SO_4, (○) heat, (●) cool.

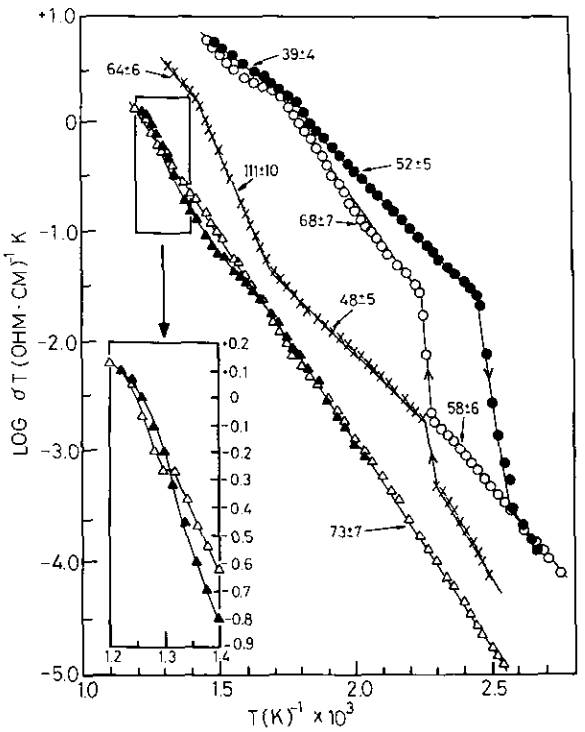

FIG. 6. Typical heat and cool mode plots of logarithm (σT) versus $T(K)^{-1}$ for Ag_2SO_4–Tl_2SO_4 system: pure Tl_2SO_4 with expanded insert, (△) heat, (▲) cool; 30 : 70 mole ratio Ag_2SO_4–Tl_2SO_4, (○) heat, (●) cool; 5 : 95 mole ratio Ag_2SO_4–Tl_2SO_4, (X) heat.

solid solution phase to the melting region with a minimum ameltrope (defined in (22)) is consistent and resembles other complex binary sulfate systems including Ag_2SO_4 (3, 21, 22). It is interesting to compare and contrast the ΔH_t versus composition plot and the subsolidus phase diagram of the Ag_2SO_4–Tl_2SO_4 system with those of the Ag_2SO_4–Rb_2SO_4 system (3) to assess their specific cation–cation interactions on the basis of ionic radius, electron configuration, mass, etc.

B. Ion Conductivity

The dependence of ionic conductivity on temperature is expressed by the Arrhenius-type equation taken from a thermodynamic formulation of the conventional transition-state theory,

$$\begin{aligned}\sigma T &= \sigma_0 \exp(-Q_c/RT) \\ &= (nq^2\lambda^2\gamma\nu/k)\exp(\Delta S^*/R - Q_c/RT),\end{aligned} \qquad [1]$$

where ν is the jump frequency of the activated mobile ion, λ is the intersite distance, γ is the intersite geometry constant, ΔS^* is the entropy of activation, Q_c is the apparent activation energy for ionic mobility, which may include a defect formation enthalpy term, and k and R are fundamental constants.

Using Eq. [1] we give typical heat and cool mode plots of $\log(\sigma T)$ versus $T(K)^{-1}$ in Figs. 5 and 6. The $\log(\sigma T)$ versus $T(K)^{-1}$ plot for $AgTlSO_4$ was reported previously (16). The discontinuities in all the σ–T heating plots correlate within ±10 K with temperatures for the corresponding phase transitions from 190°C shown in Figs. 1–3. The plot of the main σ jump at 193°C versus the system composition with its maximum at $AgTlSO_4$ (Fig. 7) paral-

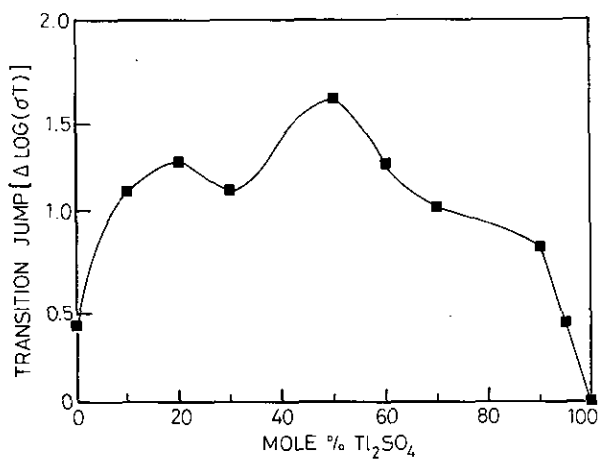

FIG. 7. Plot of the major transition jump in $\Delta\log(\sigma T)$ units versus mole % Tl_2SO_4 for the Ag_2SO_4–Tl_2SO_4 system.

lels the behavior of the $AgRbSO_4$ system. Tl_2SO_4, with conductivity of the same order of magnitude as that of Ag_2SO_4 despite the larger mass and radius of Tl^+, exhibits a barely discernible conductivity transition effect (Fig. 6) paralleling the negligible volume change at the transition, $+\Delta V \sim 0.8\%$ (21).

The heating and cooling σ–T plots of 90 : 10 Ag : Tl_2SO_4 show distinctly different profiles. The sum of the values of the cooling drop, $\Delta\log(\sigma T)$, at 335 and 147°C equals the single heating jump value, $\Delta\log(\sigma T)$, at 190°C. Also, the 5 : 95 Ag : $TlSO_4$ σ–T heating plot reveals discontinuities not evident in the DSC trace (Fig. 1). If these discontinuities represent genuine changes in structural states and are not disequilibrium measurement artifacts then ionic conductivity presents a sensitive technique for monitoring structures that are held by very weak lattice bonds. Similar behavior has been reported for a number of systems (10, 13, 15, 16, 27). These labile structures would transform undetected during analysis by diffraction techniques (24) and most likely by differential scanning calorimetry.

The cool mode σ–T plots of Ag_2SO_4-rich samples show a "proteresis" effect also observed for Ag_2SO_4–K_2SO_4, Ag_2SO_4–Rb_2SO_4, and $Na_4UO_2(SO_4)_3$, in contrast to the hysteresis of Tl_2SO_4-rich samples. The proteresis–hysteresis crossing occurs at the 60 : 40 Ag : $TlSO_4$ mole ratio with negligible effect. The data overlap for the 30 : 70 sample near 120°C contrasts with the gap between hot and cool data for the 90 : 10 sample. Does proteresis represent a genuine property of Ag_2SO_4-rich systems such as a new phase, or an artifact due to sintering of compressed sample? Proteresis resembles plastic extension in the stress/strain relationship for deformation in solids. Such deformation in this study predisposes the sample to a premature onset of the lower phase from the high α phase. Permanent deformation was observed on second heating of the 80 : 20 sample. That is, the heat and cool σ–T plots were within 10% of the initial cool plot, resembling the 90 : 10 plot (Fig. 5), with two jumps present instead of the one jump observed on the initial heating. We observed no measurable change in sample dimensions at room temperature after conductivity nor any evidence of proteresis on DSC traces.

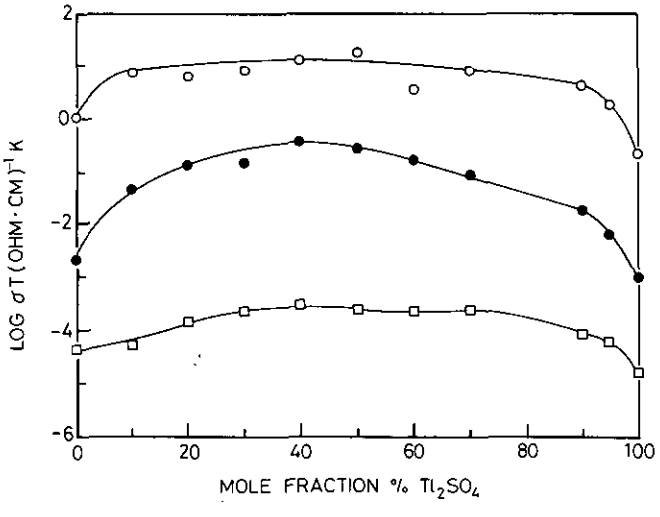

FIG. 8. Isotherm plots of logarithm (σT) versus mole % Tl_2SO_4 at (□) 127°C, (●) 217°C, and (○) 441°C.

The conductivity and Q_c values for 90 : 10 and 5 : 95 Ag : $TlSO_4$ mole ratios relative to their respective hosts (Figs. 5 and 6, respectively) provide some insight into the mode of ion transport. The constant $Q_c = 55 \pm 5$ kJ/mole for α-Ag_2SO_4 and for 90 : 10 above 420°C, one phase of assumed hexagonal α-Ag_2SO_4 structure, suggests quite strongly that higher conductivity, factor ~10, stems from a higher concentration n of activated mobile ions paralleling the 90 : 10 Ag : $RbSO_4$ behavior (3). The 5 : 95 composition with two-phase regions exhibits complex and variable behavior. The higher σ with $Q_c = 71 \pm 3$ kJ/mole below 190°C in common with β-Tl_2SO_4 suggests higher n of Tl^+ in a predominantly β-Tl_2SO_4 structure, while $Q_c = 48 \pm 3$ kJ/mole between 193 and 325°C resembles the behavior of α-$AgTlSO_4$ (3). Higher σ in the one-phase solid solution region of assumed α-Tl_2SO_4 structure above 400°C with $Q_c = 64 \pm 3$ versus 73 ± 3 kJ/mole implies greater ion mobility, μ, in a more open structure and/or higher concentration of n. The common value $Q_c = 73 \pm 5$ kJ/mole for cation mobility in the common orthorhombic structure of both Na_2SO_4 and Tl_2SO_4, in which $\sigma_{Tl_2SO_4} > \sigma_{Na_2SO_4}$ by a factor of ~10 even though $r_{Tl^+} = 164$ pm versus $r_{Na^+} = 116$ pm for CN = 6 and $m_{Tl^+}/m_{Na^+} \sim 10$, points to weaker cation–anion interaction effects or a higher degree of lattice loosening in Tl_2SO_4. In the region 325°–400°C, the interesting value $Q_c = 111$ kJ/mole, the apparent sum of 48 and 64 kJ/mole, defies clear-cut interpretation except to suggest a composite of two linked steps involving interparticle/intergranular and bulk effects in the two-phase presence.

The positive conductivity–guest-isovalent-cation composition effect in the $Tl/AgSO_4$ system as evident in the isotherms (Fig. 8) parallels the $Rb/AgSO_4$ and $Rb/NaSO_4$ systems. This behavior can originate with (i) increased n of activated mobile ions, Ag^+ and Tl^+, and possibly higher ν resulting from weaker lattice forces or lattice loosening in mixed compositions; (ii) the higher mobility μ of mobile Ag^+ in more "free" volume provided by Tl^+ presence; or a combination of (i) and (ii). The symmetric conductivity–composition profile in both one-phase and two-phase regions is in marked contrast to the asymmetric fluctuating dependence observed for the two-phase regions of Na_2SO_4–Rb_2SO_4 (2) and Ag_2SO_4–Rb_2SO_4 (3). Their relatively similar conductivities and the chemical

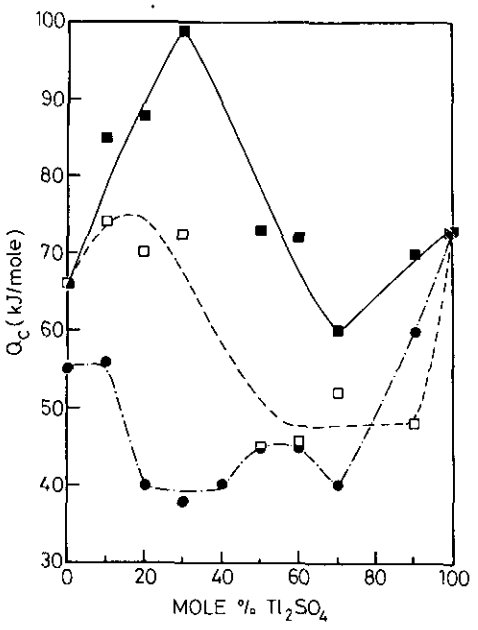

FIG. 9. Isotherm plots of activation energy Q_c versus mole % Tl_2SO_4 at (■) 127°C, (□) 217°C, and (●) 441°C.

resemblance in some aspects of Tl^+ and Ag^+ behavior can account for this smooth symmetric dependence.

Figure 9 depicts plots of Q_c against composition for three temperatures: 127°C, the lower temperature two-phase regions; 217°C, the intermediate two-phase regions above the $\beta \leftrightarrow \alpha$ $AgTlSO_4$ transition; and above 441°C, the two single solid solution regions. Ionic conductivity involves defects and its activation energy Q_c is a composite quantity consisting mainly of two terms: (i) the enthalpy of defect formation h_s, and (ii) the enthalpy of defect migration Δh_c (28). At low temperatures the fractional molar concentration of mobile cation defects is effectively constant and Q_c is identified with Δh_c while at higher temperatures h_s is included as more defects are formed. The higher Q_c values found at lower temperatures in this study do not follow the expected behavior. The constant $Q_c = 42 \pm 4$ kJ/mole at 441°C for 20–70 mole % Tl_2SO_4 in common with Q_c for the hexagonal structure of other systems (1–3, 16, 27) strongly supports a common conductivity mechanism and further suggests that h_s is zero or negligible. That is, the recurring Q_c of 45 ± 5 kJ/mole establishes the true activation energy for Ag^+ and Na^+ conductivity in the hexagonal structure with quasi-equal intersite electrostatic energy potentials. We interpret this consistent conductivity pattern in terms of a percolation-type or hopping mechanism of ion transport through a similar network of interconnected sites, i.e., similar λ and γ values in Eq. [1].

ACKNOWLEDGMENTS

The authors acknowledge financial support from the University Council of Research and the Natural Sciences and Engineering Research Council of Canada. One of us (Y.L.) is grateful to the government of the People's Republic of China for a grant-in-aid to study abroad. The solid–liquid portion of the phase diagram was determined by Dr. Anita Sharma to whom we are grateful.

REFERENCES

1. M. S. Kumari and E. A. Secco, *Can. J. Chem.* **63,** 324 (1985).
2. U. M. Gundusharma and E. A. Secco, *Can. J. Chem.* **65,** 1205 (1987).
3. Yanjia Lu, E. A. Secco, and M. G. Usha, *J. Phys. Chem. Solids* **54,** 821 (1993).
4. M. R. M. Jiang and M. T. Weller, *Solid State Ionics* **46,** 341 (1991).
5. J. O. Isard, *J. Non-Cryst. Solids* **1,** 235 (1969).
6. D. E. Day, *J. Non-Cryst. Solids* **21,** 343 (1976).
7. M. D. Ingram and C. T. Moynihan, *Solid State Ionics* **6,** 303 (1982).
8. J. M. Ziman, "Models of Disorder," Chap. 9. Cambridge Univ. Press, Cambridge, 1979.
9. R. Zallen, "The Physics of Amorphous Solids," Chap. 4. Wiley, New York, 1983.
10. U. M. Gundusharma and E. A. Secco, *Appl. Phys. A* **51,** 7 (1990).
11. M. D. Leblanc, U. M. Gundusharma, and E. A. Secco, *Solid State Ionics* **20,** 61 (1986).
12. M. R. M. Jiang and M. T. Weller, *J. Chem. Soc. Faraday Trans.* **87,** 3787 (1991).
13. G. H. Frischat, *in* "Mass Transport Phenomena in Ceramics" (A. R. Cooper and A. H. Heuer, Eds.), Mater. Sci. Res. Ser., Vol. 9, p. 285. Plenum Press, New York, 1975.
14. N. Machida and T. Minami, *J. Am. Ceram. Soc.* **71,** 784 (1988).
15. M. Tatsumisago, A. Hamada, T. Minami, and M. Tanaka, *J. Am. Ceram. Soc.* **65,** 575 (1982).
16. Yanjia Lu and E. A. Secco, *Solid State Ionics* **53–56,** 223 (1992).
17. R. D. Shannon, *Acta Crystallogr. Sect. A* **32,** 751 (1976).
18. F. A. Cotton and G. Wilkinson, "Advanced Inorganic Chemistry," 3rd ed., p. 280. Interscience, New York, 1972.
19. N. N. Greenwood and A. Earnshaw, "Chemistry of the Elements," p. 255. Pergamon, New York, 1984.
20. N. S. Dombrovskaya, *Zh. Obschch. Khim.* **3,** 293 (1933); "Phase Diagrams for Ceramists" (E. M. Levin, C. R. Robbins, and H. F. McMurdie, Eds.), No. 2882, Amer. Ceram. Soc., Columbus, OH, 1969.
21. I. N. Belayae and R. G. Kazanbekov, *Zh. Neorg. Khim.* **14,** 2553 (1969).
22. P. C. Dawson, E. A. Secco, and W. M. Oxner, *Can. J. Chem.* **67,** 1468 (1989).
23. A. J. Majumdar and R. Roy, *J. Phys. Chem.* **69,** 1684 (1965).
24. P.-N. Huang and E. A. Secco, *J. Solid State Chem.* **103,** 314 (1993).
25. M. Sahman and G. Tammamm, *Am. Phys.* **10,** 879 (1903).
26. H. Fischmeister, *Z. Phys. Chem. (Frankfurt Main)* **1,** 91 (1956).
27. K. G. MacDonald, C. MacLean, and E. A. Secco, *Can. J. Chem.* **66,** 3132 (1988).
28. I. W. Barr and A. B. Lidiard, "Physical Chemistry, an Advanced Treatise" (H. Eyring, D. Henderson and W. Jost, Eds.), p. 151. Academic Press, New York, 1970.